Effects of thickness on the piezoelectric and dielectric properties of lead zirconate titanate thin films

L. Lian and N. R. Sottos[a)]
Department of Theoretical and Applied Mechanics, University of Illinois at Urbana-Champaign, Urbana, Illinois 61801

(Received 3 August 1999; accepted for publication 11 January 2000)

Lead zirconate titanate (PZT) thin films with a Zr/Ti ratio of 52/48 were deposited on platinized silicon substrates by a sol-gel method and crystallized with preferred (111) or (100) orientation. Both the piezoelectric properties (d_{33}) and the field-induced strains of the films with different thickness and preferred orientation were measured by a laser Doppler heterodyne interferometer. The weak-field dielectric constants and dissipation factors were also measured as a function of film thickness for comparison with other work reported in the literature. The field-forced polarization switching (*P-E*) behavior was examined by Sawyer–Tower measurement. Both the piezoelectric properties and the dielectric constants of the PZT thin films were found to be strongly dependent on the film thickness. An increase in the piezoelectric constants and dielectric constants with increasing film thickness was observed for both films with preferred (111) and (100) orientations. Films with (100) preferred orientation were found to have higher piezoelectric constants and lower dielectric dissipation factors than films with (111) preferred orientation. A finite element analysis was carried out to evaluate the existing methods for determination of the d_{33} coefficient of ferroelectric thin films. The measured changes in properties with thickness were correlated with the residual stress state in the films. © *2000 American Institute of Physics.* [S0021-8979(00)03108-X]

I. INTRODUCTION

Ferroelectric ceramics have been employed extensively in a variety of sensors and actuators including strain gauges, pressure transducers, and accelerometers. Bulk ferroelectric ceramic sensors have certain shortcomings such as low fracture toughness, high inertia, and relatively large size. As a result, the range of working frequencies is limited, the dimensions are large in relation to the structure under investigation, adhesion of the piezoceramic to a structure is difficult due to different curvatures and surface roughness, and the brittleness of a piezoceramic limits the recorded vibration spectrum of the structure under investigation. Ferroelectric ceramics in thin film form have several key advantages over bulk materials as active elements in electromechanical devices. Ferroelectric thin films require a relatively low driving voltage and have small inertia, which allows for higher frequency applications. Significantly higher dielectric strengths are sustained so that higher energy densities can be achieved. Ferroelectric thin films also have a relatively rapid speed of polarization switching. New types of thin films which can achieve switching strains approaching 1% are in development. Recent applications of ferroelectric thin films include micro actuators,[1] micro sensors,[2] ultrasonic motors,[3] nonvolatile computer memories,[4] and switching capacitors for integrated circuitry.[5] Most ferroelectric thin film device development so far has focused on silicon micro-machined structures with a geometry ranging from a few to 100 μm and film thickness less than 1 μm.

The properties of ferroelectric thin films are critical to the quality and the reliability of micro-electromechanical devices. Due to their planar geometry, high deposition temperature, high residual stress state, and different structure, ferroelectric thin films are expected to behave differently from bulk ferroelectric ceramics. In order to optimize the properties and performance of thin film structures, it is essential to understand the factors that may influence the properties of the ferroelectric thin film. In recent years, extensive experimental characterization of the electric properties of ferroelectric thin films has been carried out. Udayakumar *et al.*[6] studied the thickness and temperature dependence of the electrical characteristics of lead zirconate titanate (PZT) films of morphotropic phase boundary composition fabricated using the sol-gel technique. Lakeman and Payne[7] proposed a series impedance model to explain the experimentally observed thickness effect on the dielectric properties of PZT thin films observed in experiments. Tuttle *et al.*[8] investigated the effects of orientation and residual stress on the dielectric properties of chemically prepared PZT thin films. They concluded that the sign of the film stress (tensile or compressive) at the Curie point controls the type of ferroelectric behavior of the PZT films. Garino and Harrington[9] studied the effect of stress on the dielectric properties of PZT thin films by making measurements on a film with and without the application of an external stress.

Measurement of thin film piezoelectric coefficients is challenging due to the unique geometry and small displace-

a)Author to whom correspondence should be addressed; electronic mail: n-sottos@uiuc.edu

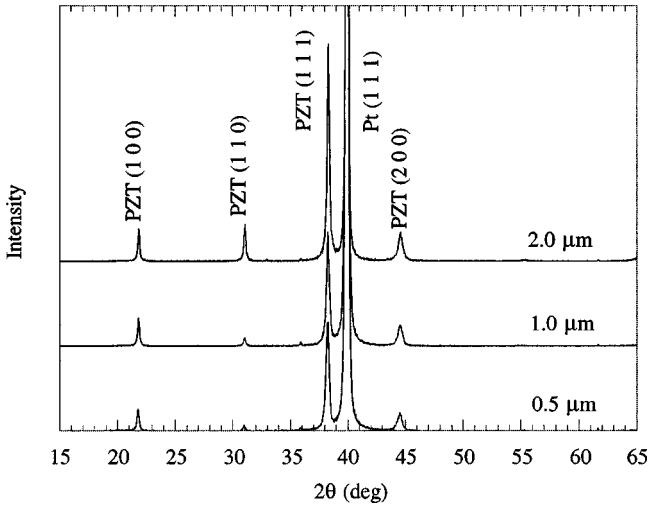

FIG. 1. X-ray diffraction pattern of PZT films with preferred (111) orientation.

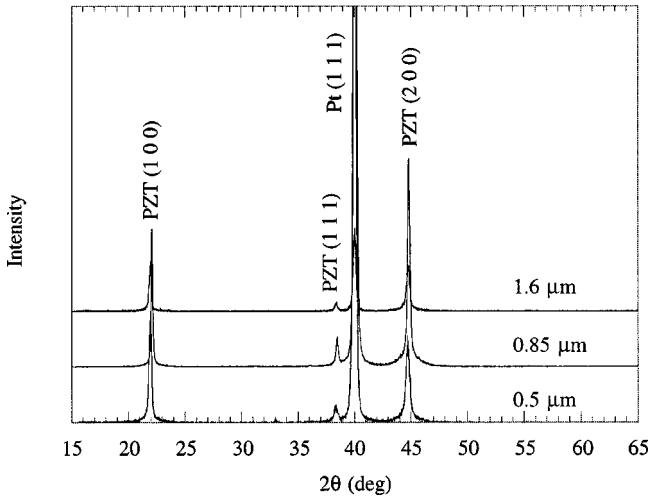

FIG. 2. X-ray diffraction pattern of PZT films with preferred (100) orientation.

ments. Traditional piezoelectric measurement techniques such as the resonance method and the strain gauge method are not suitable for films. As a result, several high resolution interferometric techniques have been adopted for characterizing thin film response. Li Moses, and Viehland[10] measured the piezoelectric properties of different ferroelectric thin films with a Michelson interferometer. Kholkin *et al.*[11] used a modified Mach–Zender interferometer to investigate the electric field, frequency, and time dependent piezoelectric response of PZT thin films. In the current article, a high resolution laser Doppler heterodyne interferometric technique is employed to quantify changes in the d_{33} piezoelectric coefficients and field-induced strains of PZT (52/48) thin films with different thickness and crystallographic orientation. Dielectric measurements on the films are also reported for comparison with other work reported in the literature. The experimental results are discussed in terms of interfacial layers and the residual stress state in the films.

II. EXPERIMENTAL PROCEDURE

A. Thin film samples

PZT thin film samples ranging from 0.5 to 2.0 μm in thickness were obtained from NZ Applied Technologies (Wolburn, MA). The composition chosen for the study was a PZT with a Zr/Ti ratio of 52/48. The films were deposited on platinized Si wafer substrates using the sol-gel technique. The crystallization behavior of the PZT thin film was examined at room temperature by x-ray diffraction (XRD, Rigku D/Max III A) and the microstructure was evaluated by scanning electron microscopy (SEM) (Hitachi S-4700 scanning electron microscope). The PZT films crystallized into a pure perovskite structure after annealing at a high temperature ranging from 650 to 750 °C. X-ray diffraction patterns revealed two different crystallographic orientations of the PZT films. As shown by the peaks in Figs. 1 and 2, one group of the films had a preferred (111) orientation and the other group of films had a preferred (100) orientation. Cross-sectional SEM photographs indicated that both groups of films had well aligned columnar grains (Fig. 3). The SEM photographs of the film surfaces revealed that the grain sizes of the films with (111) preferred orientation were more uniform and smaller [Fig. 4(a)] compared to that of the films with (100) preferred orientation [Fig. 4(b)]. No dependence of grain size on film thickness was evident in the SEM photographs. The difference in crystallographic orientations and microstructures between the two groups of PZT films may be attributed to the different properties of the sol-gel solutions or the variation in the crystal structures of the Pt/Ti layer underneath the PZT film.

Rectangular samples were cut with the width and length ranging from 1.0 to 3.0 cm. Gold electrodes of 1 mm in diameter were evaporation deposited onto the top surface of the PZT film. A portion of the PZT layer at the corner was etched away to leave the Pt layer exposed for the bottom electrode. The back surface of the Si substrate was then adhered to a block of copper as shown schematically in Fig. 5 for easy mounting and handling in the piezoelectric and dielectric measurements.

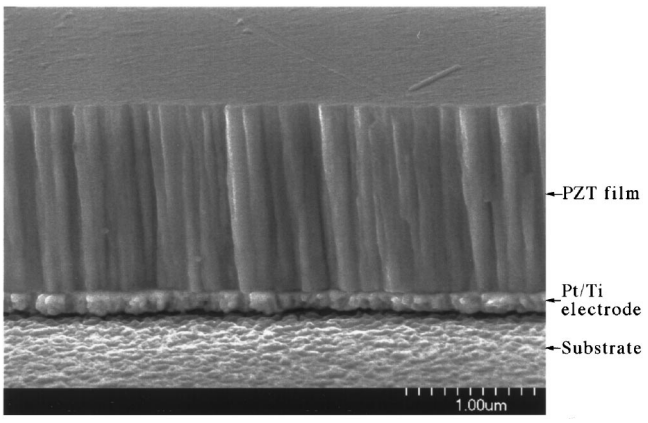

FIG. 3. SEM photomicrograph of a cross section of a PZT film with (100) preferred orientation.

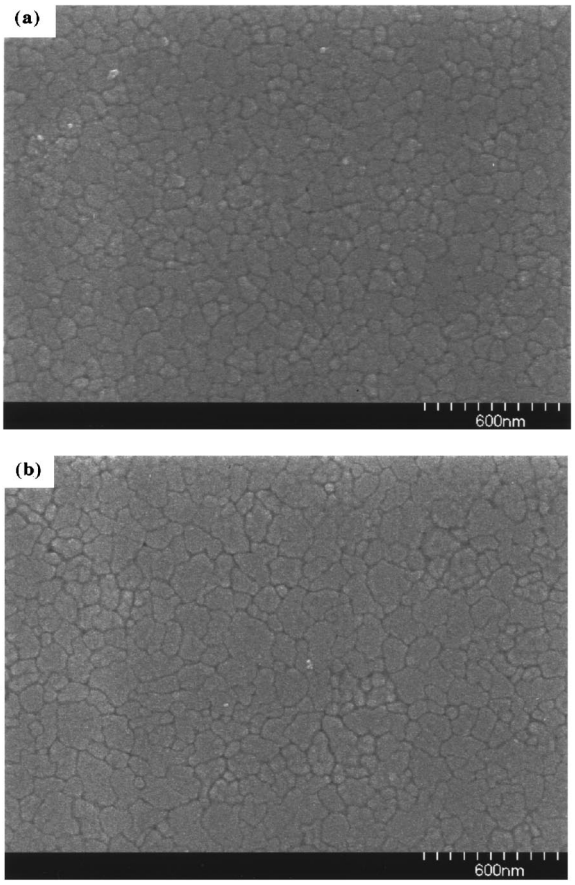

FIG. 4. SEM photomicrographs of the top PZT film surface: (a) film with (111) preferred orientation; (b) film with (100) preferred orientation.

B. Piezoelectric measurements

Due to the small thickness of the ferroelectric films, the displacements induced by an external electric field (direct piezoelectric effect) are in the angstrom range. An out-of-plane resolution of less than 1 Å is therefore required to study the low-signal piezoelectric response. As mentioned in the Introduction, this resolution can be accomplished with high sensitivity interferometric techniques. In the current investigation, a laser Doppler heterodyne interferometer was built to record the dynamic displacements of ferroelectric thin film structures over a range of frequencies.

The laser Doppler heterodyne interferometer is based on the Doppler shift effect. The Doppler frequency deviation for laser light of wavelength λ reflected normally from a moving surface at velocity v is given by the Doppler shift equation as

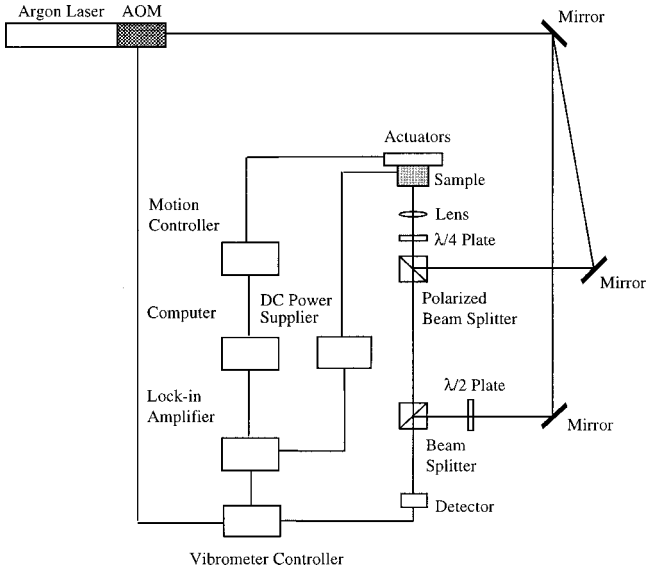

FIG. 6. Schematic of the laser Doppler heterodyne interferometer.

$$f_D = \frac{2v}{\lambda}. \tag{1}$$

The Doppler frequency deviation caused by the harmonic vibration of the sample surface is measured interferometrically and then converted to surface velocity and displacement.

A diagram of the laser Doppler heterodyne interferometer used for the dynamic displacement measurements is shown in Fig. 6. A single frequency, linearly polarized laser beam of 514.5 nm wavelength from an argon laser (Lexel Laser model 3500) is incident upon a 40 MHz acousto-optic modulator (AOM) producing two beams which are sent along different arms of the interferometer. One beam is shifted in frequency by 40 MHz and used as a reference beam. The other beam, which has the same frequency as the beam incident upon the AOM, is sharply focused at normal incidence on the sample surface. The laser beam on the sample surface has a diameter of 0.24 mm. The two beams are recombined in a beam splitter and then incident on a stationary photodetector. The intensity of the light arriving at the photodetector is expressed as

$$I = I_r + I_s + 2\sqrt{I_r I_s}\cos\left[2\pi\left(40\ \text{MHz} + \frac{2v}{\lambda}\right)t\right], \tag{2}$$

where I_r and I_s are the intensities of the reference beam and the sample beam, respectively. Any out-of-plane velocity of the sample surface produces a corresponding frequency shift

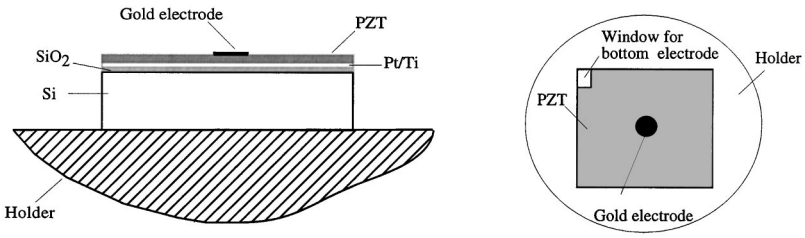

FIG. 5. Schematic of the sample for piezoelectric and dielectric measurements.

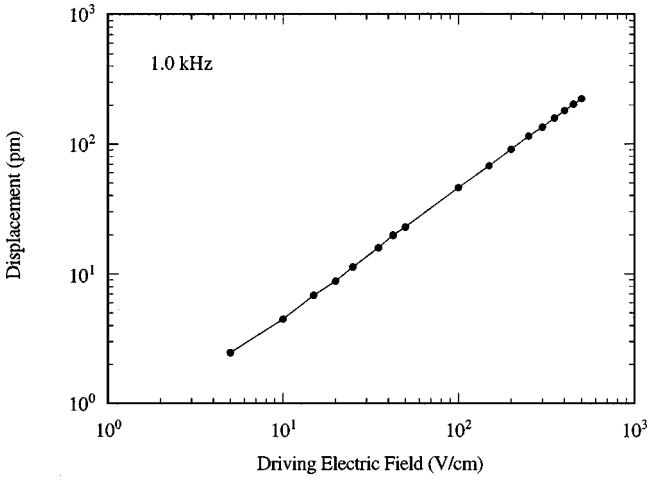

FIG. 7. Linearity of the interferometer response with driving voltage measured for *x*-cut quartz.

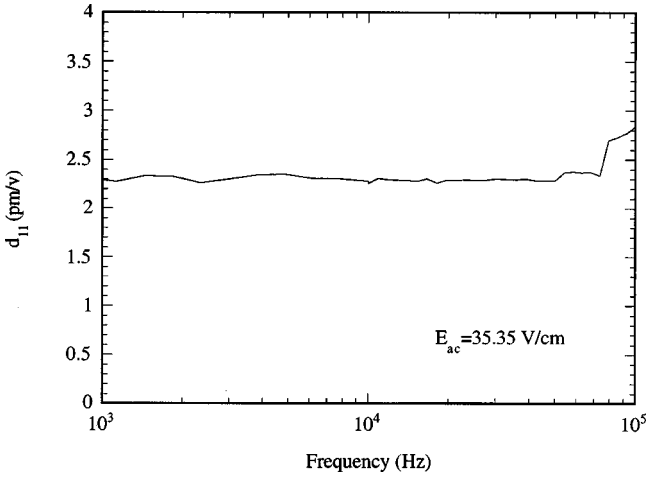

FIG. 8. Frequency dependence of the piezoelectric response measured for *x*-cut quartz.

in the signal arriving at the photodetector. The photodetector converts the intensity of the light into voltage and sends the signal to a vibrometer controller (Polytec OFV3001). The Doppler frequency shift is decoded using the frequency modulation (FM) demodulator in the vibrometer controller and produces an output voltage which is proportional to the velocity of the sample surface. A digital lock-in amplifier (Stanford Research) is then used to measure the output of the vibrometer controller. The sample is mounted onto a stage that can be moved using two actuators in order to obtain the displacement profiles. The actuators (Newport model 850B) are controlled by a microcomputer-controlled motion controller (Newport model PMC200P). Both the lock-in amplifier and the motion controller are interfaced with a Power Macintosh via the IEEE-488.2 interface.

In order to test the performance and linearity of the laser Doppler heterodyne interferometer, experiments were first done on standard *x*-cut quartz, which does not have nonlinearity in d_{11} until extremely high levels of excitation. Measurements on *x*-cut quartz samples were made in two different operational modes. In the first mode, the voltage measured by the lock-in amplifier was recorded as a function of driving voltage applied to the quartz samples at 1.0 kHz. Displacements were calculated from the output voltage and plotted in Fig. 7. Linear behavior was observed even at very low driving field. In the second operational mode, the displacement of the *x*-cut quartz was measured as a function of frequency. As shown in Fig. 8, the piezoelectric coefficient d_{11} determined from the displacement measurement remained nearly constant until the frequency approached the resonance frequency of the quartz sample, which was about 1.0 MHz. The average measured value of d_{11} at 2.27 pm/V agrees well with the published book value for quartz.

C. Dielectric measurements

The dielectric properties of the PZT thin films were measured with an LCR meter (Hewlett-Packard 4284A). The weak-field dielectric constant (K') and dissipation factor ($\tan\delta$) were measured for a driving voltage of 5 mV at 1.0 kHz at room temperature. In addition, the field-induced polarization switch (*P-E* loops) at room temperature were recorded with a modified Sawyer–Tower circuit (Radient Technologies RT-66A Standardized Ferroelectric Test System) at a frequency of 125 Hz.

III. RESULTS

A. Piezoelectric property measurements

The portion of the film between the bottom and top electrodes was first driven by an ac electric field superimposed on a dc bias. The films were not poled before the tests and the reason for the use of dc bias was to investigate the piezoelectric response of the film at different levels of polarization. The out-of-plane displacement in the thickness direction of the film was then measured using the laser Doppler heterodyne interferometer. The applied ac voltage was 1 V_{rms} for all of the samples and all of the measurements were performed at 1.0 kHz. The displacement of the film in the thickness direction was recorded as a function of the dc electric field bias which varied from -12 MV/m to $+12$ MV/m. The measured displacements of three PZT films ranging in thickness from 0.5 to 2.0 μm and with preferred (111) orientation are plotted in Fig. 9(a) as a function of dc bias. As the film thickness decreased from 2.0 to 0.5 μm, the maximum displacement decreased significantly. The displacements of three PZT films with preferred (100) orientation and ranging in thickness from 0.5 to 1.6 μm are plotted as a function of dc bias in Fig. 9(b). Again, displacement of the film decreased as the film thickness decreased. The PZT films with (100) preferred orientation had a larger piezoelectric response than the films with preferred (111) orientation at the same dc bias level for the same film thickness. In the 0.5 μm films the displacements in the (100) film were 60% larger than the (111) film at a field level of 10 MV/m.

B. Measurements of field-induced strains

Another important property of ferroelectric thin films is the polarization reversal, which results in field-induced strains. Polarization reversal is caused by the creation and

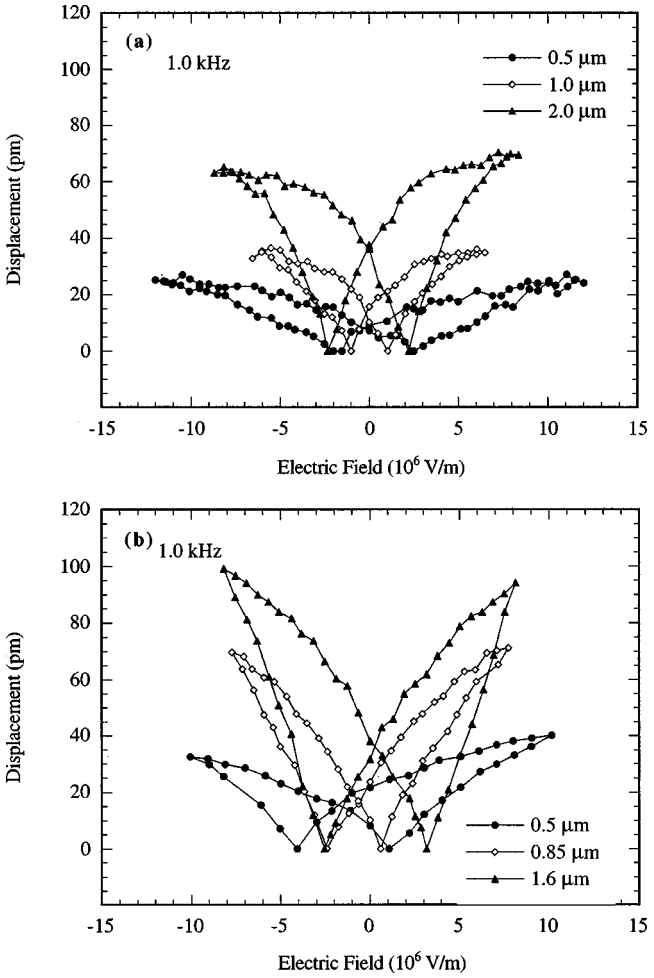

FIG. 9. Piezoelectric response of PZT (52/48) thin films as a function of dc bias: (a) film with (111) preferred orientation; (b) film with (100) preferred orientation.

subsequent motion of 90° domains under high electric field that induced significant field-induced strains. Polarization reversal is also caused by a 180° domain switch which results in significantly lower electrically induced stains than for 90° domain motion.

A large ac electric field was applied across the PZT thin film and the out-of-plane displacement was measured. Instead of using the lock-in amplifier to acquire the signal from the vibrometer controller as described previously, an averaging function of the digital oscilloscope (Tektronix TDS 420) was used to measure the time-dependent displacement of the film directly from the vibrometer output. Figure 10 shows the typical butterfly-type strain hysteresis loops for the PZT films obtained under increasing electric fields. Each loop represents an average of 10 000 cycles. Figure 11(a) shows the field-induced strains in PZT films of varying thickness with preferred (111) orientation. As the film thickness decreased from 2.0 μm to 0.5 μm, the field-induced strain also decreased. Fig. 11(b) shows the field-induced strains in PZT films with preferred (100) orientation. The field-induced strains for this orientation also decreased as the film thickness decreased. The (100) films again exhibited a larger piezoelectric response than the (111) films.

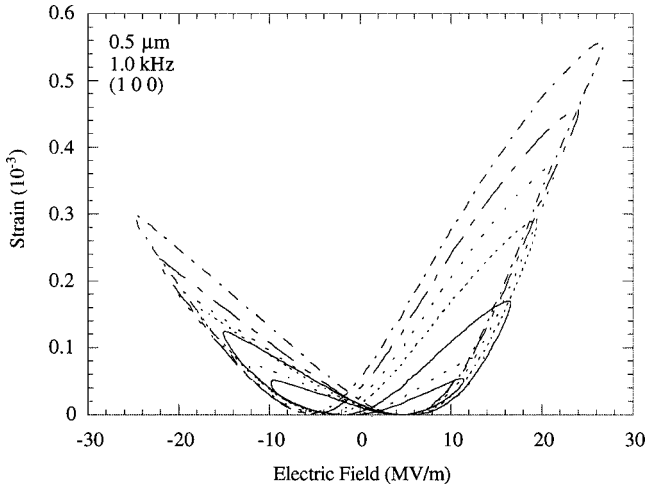

FIG. 10. Electrically induced strains in PZT (52/48) thin films under different electric field levels.

C. Dielectric measurements

Weak-field dielectric constants and dissipation factors of the PZT films with preferred (111) orientation were measured at 1.0 kHz and listed in Table I. As the film thickness decreased, the dielectric constant decreased and the dissipa-

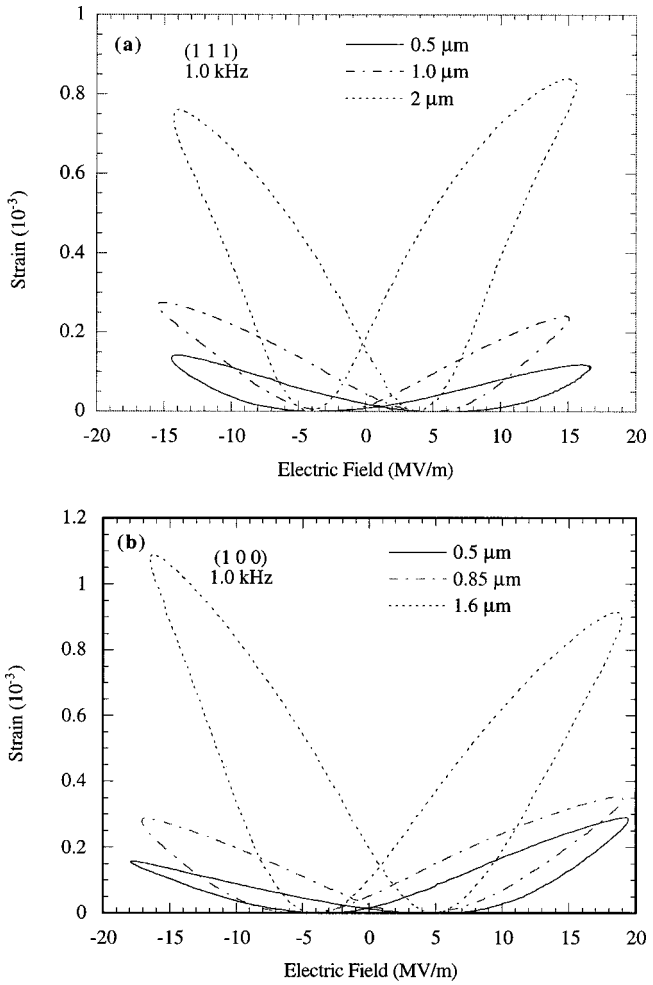

FIG. 11. Field-induced strains for various PZT(52/48) thin films: (a) film with (111) preferred orientation; (b) film with (100) preferred orientation.

TABLE I. Weak-field dielectric constants and dissipation factors of PZT (52/48) thin films with (111) preferred orientation.

Film thickness	Dielectric constant	Dissipation factor
0.5 μm	273.1	0.020
1.0 μm	538.3	0.015
2.0 μm	840.6	0.003

tion factor increased. Table II contains the weak-field dielectric constants and dissipation factors measured at 1.0 kHz for the PZT films with preferred (100) orientation. The dependence of the weak-field dielectric constant and dissipation factor is the same as that of the films with (111) preferred orientation. The dissipation factor of the film with (111) preferred orientation is higher than that of the film with (100) preferred orientation at the same thickness.

Typical hysteresis loops for the polarization switch of 0.5 μm PZT films with (111) preferred orientation and (100) preferred orientation are shown in Fig. 12. Films with (111) preferred orientation have lower values of saturation polarization and remnant polarization at zero field than films with (100) preferred orientation. The voltage available from the ferroelectric test system was not high enough to measure the saturation polarization for films thicker than 0.5 μm. As a result, a comparison of hysteresis loops for films with different thickness is not presented here. However, the value of polarization did increase with increasing film thickness at the same electric field level (below saturation) for both groups of films.

IV. DISCUSSION

A. Determination of d_{33} coefficient

The piezoelectric coefficient d_{33} of the film can be extracted from the displacement measurements presented in Sec. III B. Several different methods for calculating d_{33} from displacement data have appeared in the literature. Li, Moses, and Viehland[10] assumed that the portion of the film covered by the electrode is not laterally constrained by the remaining part of the film (not under electrode). For this case, d_{33} is calculated using the simple expression

$$d_{33}=\frac{W_z}{V}, \tag{3}$$

where W_z is the displacement of the film surface and V is the driving voltage. On the other hand, Lefki and Dormans[12] calculated d_{33} assuming that the constraint from the surrounding film is so strong that the in-plane strain is zero in the film. Under this assumption, the d_{33} coefficient is related to the out-of-plane displacement by[12]

TABLE II. Weak-field dielectric constants and dissipation factors of PZT (52/48) thin films with (100) preferred orientation.

Film thickness	Dielectric constant	Dissipation factor
0.5 μm	394.2	0.009
0.85 μm	540.8	0.004
1.6 μm	734.7	0.003

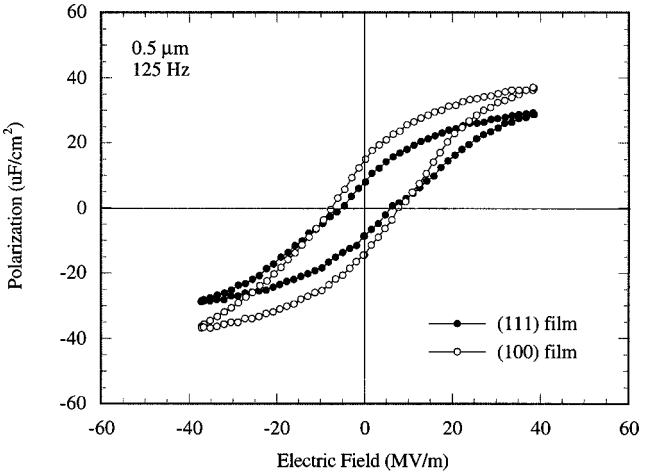

FIG. 12. Polarization-electric field hysteresis loops for 0.5 μm PZT films with (111) and (100) preferred orientations.

$$d_{33}=\frac{W_z}{V}+\frac{2d_{31}s_{13}^E}{(s_{11}^E+s_{12}^E)}. \tag{4}$$

Although Eqs. (3) and (4) provide bounds on the value of d_{33}, neither expression is strictly correct. A more detailed finite element analysis of the PZT thin film under the excitation of applied electric field was carried out to ensure the piezoelectric coefficient was evaluated correctly.

The film geometry was meshed using the preprocessing software PATRAN (MacNeal–Schwendler Corporation) and analyzed using the commercial finite element code ABAQUS (Hibbitt, Karlsson & Sorensen, Inc.). A total of 2000 eight-node biquadratic axisymmetric piezoelectric elements were used in the final mesh. A finite electrode layer was not considered in the finite element calculation because the thickness of the electrode was negligible compared with that of the film. Effects of the electrode were introduced through the boundary conditions at the top surface of the film. Since the elastic material constants of PZT thin films are not well characterized, the properties of bulk PZT (52/48) were used in the calculation (Table III). Some preliminary measurements of d_{31} for the films were made in our lab using a cantilever beam sample (film+substrate). The beams were driven with an electric field and the out-of-plane tip deflection was measured interferometrically. Using an established bimorph analysis,[13] a value of -33.9 pm/V for d_{31} was obtained,

TABLE III. Material properties of bulk PZT (52/48).[a]

d_{31} (10^{-12} C/N)	-93.5
d_{33} (10^{-12} C/N)	223
d_{15} (10^{-12} C/N)	494
s_{11}^E (10^{-12} m^2/N)	13.8
s_{33}^E (10^{-12} m^2/N)	17.1
s_{12}^E (10^{-12} m^2/N)	-4.07
s_{13}^E (10^{-12} m^2/N)	-5.8
s_{44}^E (10^{-12} m^2/N)	48.2
s_{66}^E (10^{-12} m^2/N)	38.4
K_1^T	1180
K_3^T	730

[a]See Ref. 18.

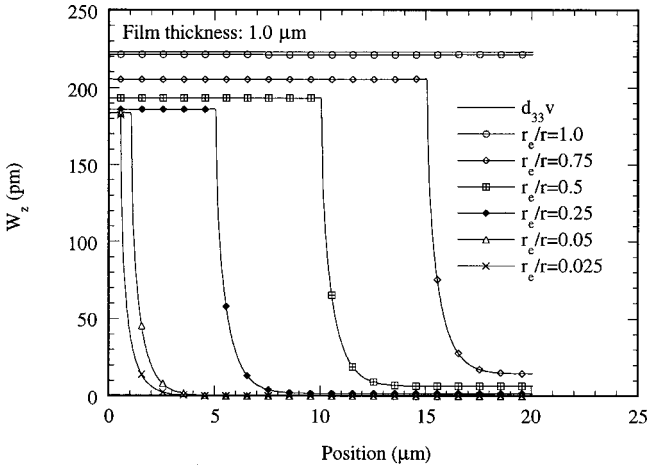

FIG. 13. Displacement profiles at different electrode radius to sample radius ratios (r_e/r).

which is about one third of the value of bulk PZT(52/48). This value was used in all the finite element calculations. The predicted displacement profiles of a 1.0-μm-thick PZT thin film are plotted in Fig. 13 for different electrode radius to sample radius ratios (r_e/r). In all cases, the displacement profile of the film is uniform under the electrode and rapidly decays away from the electrode. Figure 14 shows the dependence of the displacement at the center of the 1.0-μm-thick film on the value of r_e/r. As the size of the electrode decreases, the displacement of the film also decreases until r_e/r approaches a constant value, which depends on the properties of the film. As the electrode size continues to decrease, the displacement of the film remains nearly constant. The limit of the film displacement is much higher than the estimation made under Lefki and Dormans' assumption [Eq. (4)] but lower than the estimation made by Li, Moses, and Viehland [Eq. (3)]. Equation (3) provides a lower bound estimation for the d_{33} coefficient of the thin film while Eq. (4) predicts an upper bound. Since the electrode sizes were small compared to the entire sample surface, the actual d_{33} value will lie somewhere between the two predictions. The d_{33} coefficients of the PZT thin films at a dc bias level of 5 MV/m calculated from Eq. (3), Eq. (4), and finite element (FE) analysis are listed in Tables IV and V. Compared with the FE predictions, Eq. (3) provides a better estimation of the d_{33} coefficient than Eq. (4). For both the (100) and the (111) films, the calculated d_{33} values decrease significantly with decreasing film thickness. Furthermore, the maximum value

TABLE IV. Estimation of the d_{33} coefficient of the PZT (52/48) films with (111) preferred orientation at a dc bias level of 5 MV/m. Note: $d_{31} = -33.9$ pm/V, $r_e/r = 0.05$.

	d_{33} (pm/V)		
Film thickness	$\frac{W_z}{v}$	FE	$\frac{W_z}{v}+\frac{2d_{31}s_{13}^E}{(s_{11}^E+s_{11}^E)}$
0.5 μm	12.4	13.2	57.6
1.0 μm	24.6	26.3	65.0
2.0 μm	46.0	49.1	86.4

TABLE V. Estimation of the d_{33} coefficient of the PZT (52/48) films with (100) preferred orientation at a dc bias level of 5 MV/m. Note: $d_{31} = -33.9$ pm/V, $r_e/r = 0.05$.

	d_{33} (pm/V)		
Film thickness	$\frac{W_z}{v}$	FE	$\frac{W_z}{v}+\frac{2d_{31}s_{13}^E}{(s_{11}^E+s_{12}^E)}$
0.5 μm	23.1	24.7	63.5
0.85μm	43.1	46.1	83.5
1.6 μm	57.2	61.1	97.5

of d_{33} for the thickest (100) film at a dc bias of -8.2 MV/m is 75.8 pm/V, only 34% of the value reported for bulk PZT of the same composition (Table III). Possible explanations for this behavior are discussed below.

B. Residual stress effects

The measurements presented in Sec. III demonstrate that both piezoelectric properties and dielectric properties of PZT thin films depend strongly on film thickness. Several authors[14–17] have reported that residual stress changes with film thickness and hypothesized that it may have a significant effect on the piezoelectric and dielectric film properties. Significant residual stresses build up in the ferroelectric thin film structures during the fabrication process. The total residual stress (σ^t) developed in the thin film during fabrication consists of three parts

$$\sigma^t = \sigma^i + \sigma^{\text{th}} + \sigma^e, \tag{5}$$

where σ^i, σ^{th}, σ^e are the intrinsic stress, the thermal stress, and the extrinsic stress, respectively. The intrinsic stress is induced by the formation of the grain boundaries as the crystal grain grows and interacts with neighboring grains, by the shrinkage due to water and solvent evaporation and decomposition and pyrolysis of nonvolatile organic species during heat treatment, and by the phase transformation at the transition temperature. Thermal stress is induced by the mismatch between thermal expansion coefficients of the ferroelectric film and the substrate. The extrinsic stress originates

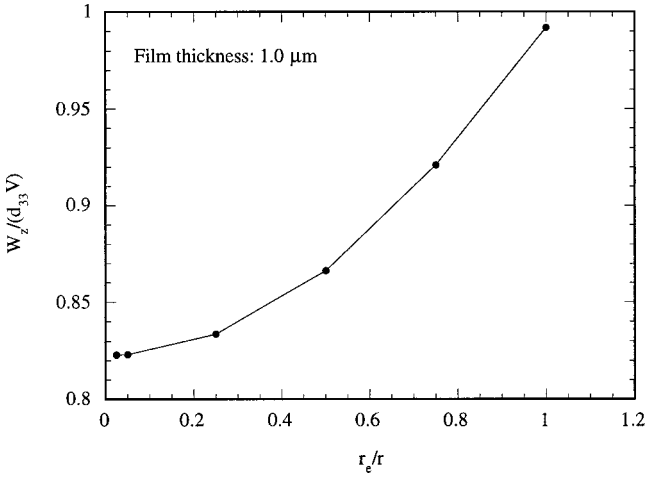

FIG. 14. Displacement of the films as a function of (r_e/r).

from the lattice parameter mismatch between the film and the substrate. Spierings *et al.*[14] found that the residual stresses in both the sputter deposited platinum electrodes and sol-gel deposited PZT films on silicon substrates were tensile and of the order of 1 GPa and 100 MPa, respectively.

Several techniques have been used for the determination of stresses in thin films. These include x-ray diffraction, optical fluorescence, and wafer curvature measurement. Wafer curvature measurement is the most widely used of the three methods. Sengupta *et al.*[15] investigated the stress development in sol-gel derived PT thin layers by measuring the wafer curvature using a laser reflectance method. The stress was then calculated according to the Stoney equation. They found that the tensile stress in the film decreased as the number of layers increased. After a critical number of layers were deposited, the stress became compressive. Garino and Harrington[9] observed that a decrease of the tensile stress in the film led to an increase in the dielectric constants. Hence, changes in the residual stress state with film thickness might be one major cause for the increasing piezoelectric properties and dielectric constants with increasing film thickness observed in the current experiments.

Residual stresses are also closely related with the crystallographic orientations in the films. Tuttle *et al.*[8] observed that the sign of the film stress at the Curie point controls the orientation of the domain structure in PZT thin films. Compressive stresses on cooling through the Curie point result in domains with their ''*c*'' direction normal to the film surface, while tensile stresses result in domains with their ''*a*'' direction normal to the thin layer. On the other hand, films with different crystallographic orientations may have different in-plane material properties because of the property-orientation behavior of perovskite single crystals, different microstructural features [Figs. 4(a) and 4(b)] and different grain interactions. Hence, the residual stresses in the films may also be different. The residual stresses in films with (111) preferred orientation may be larger than those in films with (100) preferred orientation, which leads to lower piezoelectric response, higher dielectric dissipation factor, and lower value of saturation polarization.

C. Interfacial layer and grain size effects

In addition to residual stress, the presence of a thin layer with a low dielectric constant can also have a large effect on the net dielectric constant of the film.[7] The interaction between the film and the top/bottom electrode lead to the existence of interlayers. The interlayer may also alter the distribution of the electric field in the PZT film which will influence both the net piezoelectric properties and the magnitude and shape of the electrically induced strain hysteresis loop. The thinner the film, the more significant the interlayer effect. Jang *et al.*[17] also found the grain size to be dependent on thickness in $BaTiO_3$ ferroelectric films. They correlated the observed thickness dependence of film properties with change in the grain size. However, SEM photographs of the films used in this study do not show any significant dependence of grain size on film thickness.

V. CONCLUSIONS

PZT thin films with Zr/Ti ratio of 52/48 deposited onto platinized silicon wafers using sol-gel techniques were studied. Both the film thickness effect and crystallographic orientation effect were investigated. The piezoelectric response including the d_{33} piezoelectric constant and the field-induced strain hysteresis loops of the films were measured using a laser Doppler heterodyne interferometer. The dielectric properties of the films were measured for comparison with other work reported in the literature. The results are summarized as follows:

(1) The piezoelectric coefficients d_{33}, the field-induced strains, and the weak-field dielectric constants of the PZT film decrease with film thickness.
(2) The dissipation factor increases with decreasing film thickness.
(3) Films with (100) preferred orientation have higher piezoelectric coefficients d_{33}, smaller dissipation factor, and higher saturation and remnant polarizations than films with (111) preferred orientation.

The thickness and crystallographic orientation dependence of the film properties are attributed to several factors. The most important factor is the residual stress in the film which depends on film thickness and processing conditions. Interfacial layers between the film and the electrodes may also contribute to the thickness effects.

ACKNOWLEDGMENTS

This work was supported by the National Science Foundation under Grant No. NSF CMS 95-32038. The authors would like to acknowledge helpful conversations with Professor David Payne and Ryan Ong in the Department of Material Science and Engineering at the University of Illinois at Urbana-Champaign. The authors also thank Xinliang Lu for his help in performing the dielectric measurements. The authors acknowledge the use of the facilities in the Center for Microanalysis in the Material Research Laboratory at the University of Illinois.

[1] E. S. Kim and R. S. Muller, IEEE Electron Device Lett. **EDL-7**, 254 (1987).
[2] S. W. Wenzel, and R. M. White, IEEE Trans. Electron Devices **ED-35**, 735 (1988).
[3] R. M. Morney, R. M. White, and R. T. Howe, Proceedings of the IEEE Ultrasonics Symposium, Montreal, 1989, p. 745.
[4] D. Bondurant and F. Gnadinger, IEEE Spectr. **30**, 30 (1989).
[5] M. H. Frey and D. A. Payne, Appl. Phys. Lett. **63**, 2753 (1993).
[6] K. R. Udayakumar, P. J. Schuele, J. Chen, S. B. Krupanidhi, and L. E. Cross, J. Appl. Phys. **77**, 3981 (1995).
[7] C. D. E. Lakeman and D. A. Payne, Ferroelectrics **152**, 145 (1994).
[8] B. A. Tuttle, J. A. Voigt, T. J. Garino, D. C. Goodnow, R. W. Schwartz, D. L. Lamppa, T. J. Headley, and M. O. Entongh, ISAF'92. Proceedings of the Eighth IEEE International Symposium on Applications of Ferroelectrics 1992, p. 344.
[9] T. J. Garino and M. Harrington, Mater. Res. Soc. Symp. Proc. **243**, 341 (1992).
[10] J. Li, P. Moses, and D. Viehland, Rev. Sci. Instrum. **66**, 215 (1995).
[11] A. L. Kholkin, Ch. Wütchrich, D. V. Taylor, and N. Setter, Rev. Sci. Instrum. **67**, 1935 (1996).

[12] K. Lefki and G. J. M. Dormans, J. Appl. Phys. **76**, 1764 (1994).
[13] J. G. Smits and Wai-shing Choi, IEEE Trans. Ultrason. Ferroelectr. Freq. Control **38**, 256 (1991).
[14] G. A. C. M. Spierings, G. J. M. Dormans, W. G. J. Moors, M. J. E. Ulenaers, and P. K. Larsen, J. Appl. Phys. **78**, 1926 (1995).
[15] S. S. Sengupta, S. M. Park, D. A. Payne, and L. H. Allen, J. Appl. Phys. **83**, 2291 (1998).
[16] J. Lappalainen, J. Frantti, and V. Lantto, J. Appl. Phys. **82**, 3469 (1997).
[17] J. W. Jang, S. J. Chung, W. J. Cho, T. S. Hahn, and S. S. Choi, J. Appl. Phys. **81**, 6322 (1997).
[18] B. Jaffe, W. Cook, and H. Jaffe, *Piezoelectric Ceramics* (Academic, London, 1971).